Sensors and Materials, Vol. 30, No. 10 (2018) 2359–2367
MYU Tokyo

S & M 1681

H_2O_2 Detection by Redox-based Potentiometric Sensors under Biological Environments

Tatsuya Iwata,[1,2*] Sinya Mizutani,[1] Koichi Okumura,[1]
Yuki Okumura,[1] Kazuhiro Takahashi,[1,2] and Kazuaki Sawada[1,2]

[1]Department of Electrical and Electronic Information Engineering,
Toyohashi University of Technology,
1-1 Hibarigaoka, Tempaku-cho, Toyohashi, Aichi 441-8580, Japan
[2]Electronics-Inspired Interdisciplinary Research Institute,
1-1 Hibarigaoka, Tempaku-cho, Toyohashi, Aichi 441-8580, Japan

(Received April 2, 2018; accepted September 7, 2018)

Keywords: potentiometry, redox sensors, neurotransmitters, H_2O_2

Hydrogen peroxide (H_2O_2) is an important target material for detecting biomolecules including acetylcholine (ACh), glutamate (Glu), and glucose. In this study, we report on H_2O_2 detection under biological environments based on the redox reaction. The redox potential change caused by the reaction between the electron mediators of ferrocenes and H_2O_2 catalyzed by horseradish peroxidase (HRP) was measured using a gold electrode connected to a source follower circuit. The mediators were either dissolved in sample solutions using ferrocenyl methanol (FcMeOH) or immobilized on the sensor surface in the form of 11-ferrocenyl-1-undecanethiol (11-FUT). H_2O_2 detection under biological environments was demonstrated in both samples. The overall outputs in the 11-FUT-immmobilzed electrodes were lower than those in the samples with dissolved FcMeOH. The detection range of H_2O_2 was from 10^{-5} to 10^{-3} M for the samples with dissolved FcMeOH, while it was from 10^{-4} to 10^{-2} M for the 11-FUT-immobilized electrodes. It was suggested that the oxidation of the mediators by H_2O_2 insufficiently took place in the 11-FUT-immobilized electrodes, leading to the lower outputs.

1. Introduction

Electrochemical sensors[(1)] have been extensively studied with the aim of realizing miniature and simple biosensing systems. Recently, bioimaging based on electrochemical methods[(2–4)] has been attracting attention because of its label-free detection. Electrochemical sensors are roughly divided into amperometry[(4–7)] and potentiometry.[(8–10)] In principle, the output of potentiometric sensors does not change with the sensing area, and thus they are attractive for image sensors, for which miniature sensing areas are required to achieve high-resolution imaging.

Various neurotransmitters and biomolecules have been detected by potentiometric techniques including ion-sensitive field-effect transistors[(8)] and charge-transfer-type

*Corresponding author: e-mail: iwata@ee.tut.ac.jp
https://doi.org/10.18494/SAM.2018.1947

ISSN 0914-4935
https://myukk.org/

potentiometric sensors.[10] For example, the detection of acetylcholine (ACh),[11–13] glutamate (Glu),[14] and glucose[12,15] has been reported, and they were detected as pH changed with enzymatic reactions. In biological environments, however, it is necessary to use pH buffers, which suppress pH changes caused by enzymatic reactions, resulting in a reduction in the magnitude of output signal. On the other hand, the detection of target molecules based on the changes in redox potential of working electrodes has been reported.[16–18] In these studies, target molecules were degraded by enzymes, and, at the same time, mediators included in the specimen were oxidized/reduced. Then, the redox potential determined by the quotient of the oxidation state of the mediators was detected by FETs. In our previous study, we reported the detection of hydrogen peroxide (H_2O_2) based on the redox potential in the system consisting of a gold electrode and a source follower circuit.[19] A number of biomolecules (e.g., ACh, Glu, and glucose) generate H_2O_2 when they are degraded by enzymes, and H_2O_2 acts as an oxidant. Thus, H_2O_2 is a useful material for detecting these molecules based on the redox mechanism.

Although we reported the detection of H_2O_2 by a potentiometric technique in our previous study, the demonstration under biological environments has not been realized yet. In addition, the effects of the device structure including the immobilization of the mediators are yet to be investigated. Thus, in this study, potentiometric sensors with mediator-immobilized electrodes were fabricated, and the response of the electrode potential to H_2O_2 was investigated under biological environments.

2. Experimental Procedure

2.1 Sensing principle

Ferrocenes were employed as electron mediators. The redox reaction between H_2O_2 and ferrocenes was catalyzed using horseradish peroxidase (HRP) as described in the following equations:

$$H_2O_2 + 2H^+ + 2e^- \xrightarrow{\text{HRP}} 2H_2O, \tag{1}$$

$$2\text{Ferrocene (red)} \rightarrow 2\text{Ferrocene (ox)} + 2e^-, \tag{2}$$

where "red" and "ox" indicate the reduced and oxidized states of ferrocenes, respectively. The resulting electrode potential (E) is determined by the quotient of the concentration in each of these states as

$$E = E^{\circ} + \frac{RT}{nF} \ln \frac{[\text{Ferrocene (ox)}]}{[\text{Ferrocene (red)}]}, \tag{3}$$

where E° is the standard potential, R is the gas constant, T is the temperature, n is the number of electrons involved in the reaction (two in this study), and F is the Faraday constant. If all of the ferrocenes are initially in the reduced state, the concentration of ferrocenes in the oxidized state

corresponds to the generated/added H_2O_2 concentration, and thus the output corresponding to the concentration of H_2O_2 is obtained.

2.2 Materials

As described in the previous section, HRP and electron mediators were used to detect H_2O_2, where both ferrocenyl methanol (FcMeOH) and 11-ferrocenyl-1-undecanethiol (11-FUT) were employed as electron mediators. To mimic biological environments, a recording medium (RM) composed of 135 mM NaCl, 5 mM KCl, 2 mM $CaCl_2$, 1 mM $MgCl_2$, 10 mM d-glucose, and 10 mM sodium 4-(2-hydroxyethyl)piperazine-1-ethanesulfonate (HEPES) (pH 7.4) was employed. The RM was prepared by dissolving these substances in deionized water (DIW) (18.2 MΩ·cm at 298 K). H_2O_2 and other substances were dissolved in the RM to prepare sample solutions unless otherwise noted. HRP and FcMeOH (95%) were purchased from Sigma-Aldrich Inc. Sodium HEPES (≥99.0%) was purchased from Dojindo Laboratories. NaCl, KCl, $MgCl_2$, ethanol (99.5%), H_2O_2 (30.0%), potassium hexacyanoferrate(II) trihydrate [$K_4Fe(CN)_6$] (99.5%), and potassium hexacyanoferrate(III) [$K_3Fe(CN)_6$] (99.0%) were purchased from Wako Pure Chemical Industries, Ltd. Ethanol was used as a solvent for both FcMeOH and 11-FUT solutions. $K_4Fe(CN)_6$ and $K_3Fe(CN)_6$ were used to examine the electrochemical characteristics of the measurement system.

2.3 Device fabrication

Gold (Au) electrodes were fabricated as reported in Ref. 19. An approximately 300-nm-thick Au film was deposited by sputtering. Each of the electrodes was patterned into a 1 × 1 mm^2 area by a conventional lift-off technique. Both electrodes modified with 11-FUT and without modification were prepared as schematically illustrated in Fig. 1(a). The modification was conducted in the following procedure according to Ref. 18. First, the electrodes were cleaned using a mixture of sulfuric acid (H_2SO_4) and hydrogen peroxide (H_2O_2) at a ratio of 3:1 (SPM) to remove organic substances from the Au surface. The cleaning was performed with 50 μL of SPM for 5 min, followed by rinsing with DIW for about 1 min. Then, the gold electrodes were immersed in 0.5 ml of a 0.5 mM 11-FUT solution for 24 h at room temperature to immobilize 11-FUT on the gold surface. Finally, they were rinsed with ethanol and DIW to remove the unreacted 11-FUT.

2.4 Measurement procedure

The electrode potential of the Au electrode was measured with a source follower circuit consisting of an off-chip n-channel metal-oxide-semiconductor FET (MOSFET), a voltage source, and a current source. The MOSFET was fabricated using our facility, and the dimension of the gate was length/width = 10/40. The MOSFET chip is described in detail elsewhere.[19] Figure 1(b) shows a schematic of the measurement system. A constant current (I_S) and constant voltages (V_{REF} and V_D) were provided by a semiconductor device analyzer (SDA) (B1500A,

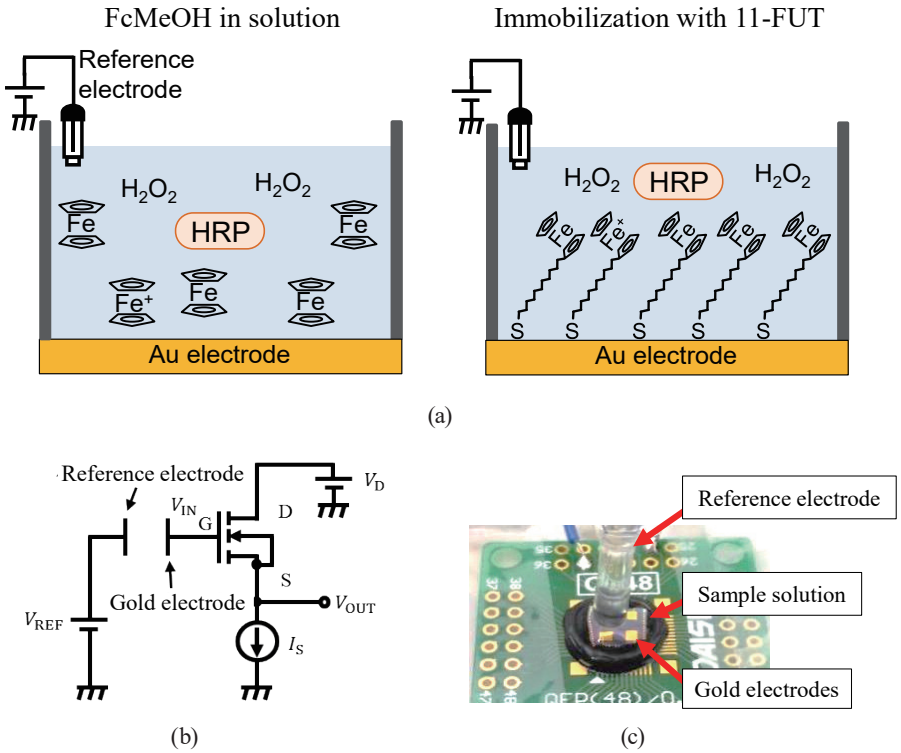

Fig. 1. (Color online) Schematic illustration of the (a) redox-reaction system and (b) measurement circuit. (c) Photograph of the electrode chip.

Agilent Technologies). The common ground was connected to that of the SDA. A metal shield box was used for electromagnetic and light shielding. The characteristics of the source follower circuit are shown in Fig. 2. Because the constant current was supplied by the SDA, its gain was nearly unity. The gold electrode, a Ag/AgCl reference electrode with 3 M NaCl, and the MOSFET were put in the metal shield box. A picture of the electrode chip is shown in Fig. 1(c). During the measurements, a couple of cups containing water were put in the shield box to suppress the evaporation of the sample solution. In the measurement system, the output (V_{OUT}) is described by the following equation:

$$V_{OUT} = V_{IN} - (V_T + K), \tag{4}$$

$$V_{IN} = V_{REF} + (E_{\mathrm{Au}} - E_{\mathrm{AgCl}}), \tag{5}$$

where V_{IN} is the gate voltage of the MOSFET, V_T is the threshold voltage of the MOSFET, K is the constant related to the drain current, and V_{REF} is the voltage of the AgCl/Ag electrode. E_{Au} and E_{AgCl} are the interfacial potentials between each of these electrodes and the electrolyte. Consequently, V_{OUT} is expressed as

$$V_{OUT} = E_{\mathrm{Au}} - E_{\mathrm{AgCl}} + (V_{REF} - V_T - K). \tag{6}$$

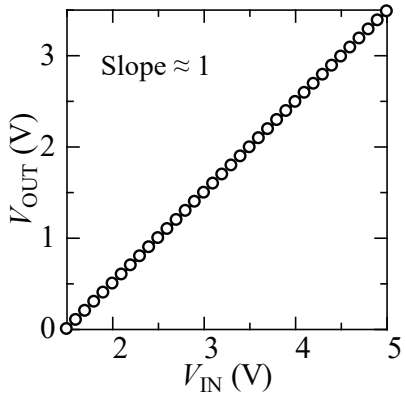

Fig. 2. Output characteristics of the source follower circuit. The slope of the characteristics, namely, the output gain, is nearly unity.

Because the parameters in parentheses were constant throughout the measurements, the data shown hereafter refer to the difference in the interfacial potential of electrodes ($E_{Au} - E_{AgCl}$).

First, to examine the measurement principle, the dependence of the electrode potential on redox compounds was measured on the basis of the procedure described in Ref. 16. The gold electrode and the Ag/AgCl reference electrode with 3 M NaCl were immersed in 100 µl of the mixed solutions of $K_4Fe(CN)_6$ and $K_3Fe(CN)_6$ at various ratios. They were dissolved in the RM, while the total concentration of the mixed solutions was maintained at 10 mM. The response of the gold electrodes to pH was also measured. The gold electrode and the Ag/AgCl reference electrode with 3 M NaCl were immersed in 100 µL of pH buffer solutions containing sodium dihydrogen phosphate (NaH_2PO_4) and disodium hydrogen phosphate 12-water ($Na_2HPO_4{\cdot}12H_2O$). The pHs of the prepared buffer solutions were 5.8, 6.8, and 7.8.

The changes in the potential of the gold electrodes for H_2O_2 were obtained by the following procedure. The electrodes and the Ag/AgCl reference electrode with 3 M NaCl were first immersed in 90 µL of RM and the measurement was started. After waiting for 280 s from the measurement start to confirm the stability of the potential, the shield box was opened, and then 10 µl of H_2O_2 solution was added at 300 s. The potential was measured for 1200 s after the H_2O_2 addition. Besides the electrode modified by 11-FUT, the potential was also measured for unmodified gold electrodes with an RM containing 2 mM FcMeOH to investigate the influences of the immobilization of the electron mediators.

3. Results and Discussion

3.1 Response of gold electrodes to redox potential and influences of pH

According to the redox mechanism described in Sect. 2.1, the change in electrode potential should be proportional to the logarithm of the concentration ratio of $K_3Fe(CN)_6$ to $K_4Fe(CN)_6$ as shown in Eq. (7), where brackets indicate the concentrations of the corresponding substances. The electrode potential against the Ag/AgCl electrode for various quotients between $[K_3Fe(CN)_6]$

and $[K_4Fe(CN)_6]$ is plotted in Fig. 3. The potential increases with increasing concentration ratio of $K_3Fe(CN)_6$ to $K_4Fe(CN)_6$, and the relationship between the potential and the logarithm of $[K_3Fe(CN)_6]/[K_4Fe(CN)_6]$ exhibits good linearity in the range from 10^{-2} to 10^2, while there are discrepancies between the measured values and the fitted line for the concentration ratio near 10^{-3} and 10^3. In the ranges, the concentrations of $[K_3Fe(CN)_6]$ and $[K_4Fe(CN)_6]$ are low, and thus the errors in the concentration or volume of the solution may not be negligible to cause such discrepancies. The extracted slope for the range was approximately 54.7 mV/dec, which is near the Nernstian value (59.1 mV at 298 K). The results corroborate that the fabricated sensor detects the electrode potential determined by redox equilibrium.

$$E = E^{\circ} + \frac{RT}{nF}\ln\frac{\left[K_3Fe(CN)_6\right]}{\left[K_4Fe(CN)_6\right]} \approx E^{\circ} + 59.1\,\mathrm{mV}\log\frac{\left[K_3Fe(CN)_6\right]}{\left[K_4Fe(CN)_6\right]}\ (\text{at } 298\ \mathrm{K}) \tag{7}$$

The responses of the electrodes to pH were also measured. The electrode potential in solutions with various pHs is shown in Fig. 4, where error bars indicate standard deviations (n = 3). Although there are large deviations, the electrode potential is confirmed to be insensitive to pH.

3.2 Responses of electrodes to hydrogen peroxide

Figure 5 shows the time-dependent H_2O_2 response of the electrode potential for which FcMeOH was dissolved in the sample solution. A solution containing H_2O_2 was added at 300 s. In the figure, the responses for various H_2O_2 concentrations including the control sample (without H_2O_2 addition) are plotted. The output drift was approximately 20 mV for 1200 s after H_2O_2 addition. For the H_2O_2 concentration of 10^{-6} M and below, the potential change by H_2O_2 was less than or comparable to the magnitude of the drift. In contrast, a significant potential change was observed for the H_2O_2 concentration of 10^{-5} M, and the output increased with increasing

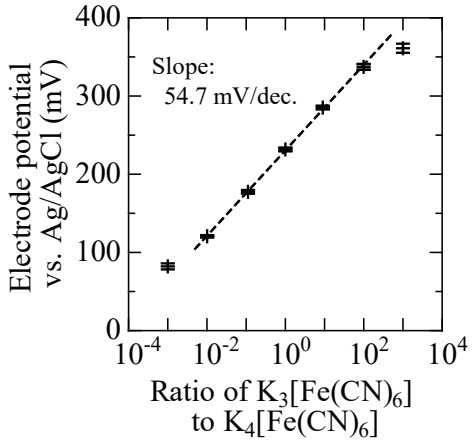

Fig. 3. Electrode potential as a function of the concentration ratio of $K_3Fe(CN)_6$ to $K_4Fe(CN)_6$.

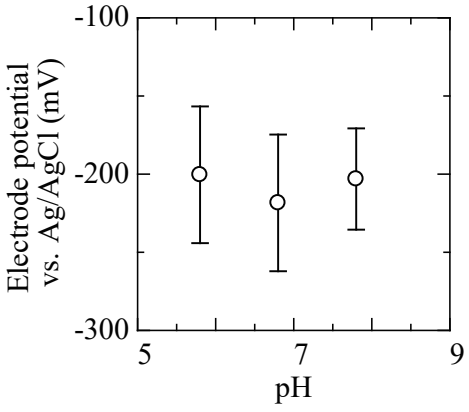

Fig. 4. Electrode potential as a function of pH.

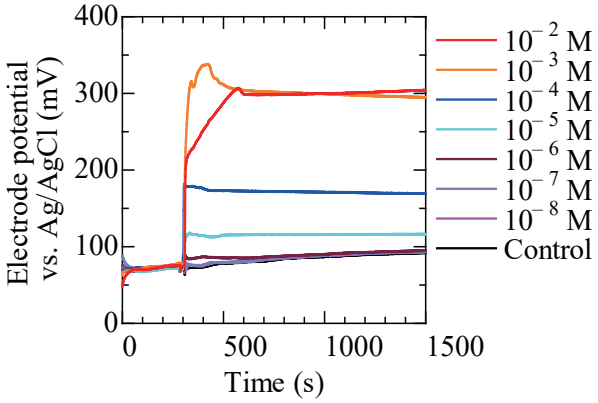

Fig. 5. (Color online) Time dependence of the electrode potential in response to the addition of H_2O_2 solution at various concentrations, where FcMeOH was dissolved in the solution, not immobilized on the electrode surface. In the figure, the H_2O_2 solution was added at 300 s.

H_2O_2 concentration. Further increasing the H_2O_2 concentration to more than 10^{-3} M resulted in output saturation.

The time-dependent H_2O_2 response of the electrode on which 11-FUT was immobilized is shown in Fig. 6. In a similar manner to Fig. 5, the H_2O_2-containing solution was added at 300 s. The electrode potential was hardly changed for the H_2O_2 concentration of 10^{-5} M and below, and it was increased for the H_2O_2 concentration of 10^{-4} M and above. In contrast to the sample with dissolved FcMeOH, the potential in the steady state further increased even for above 10^{-2} M H_2O_2. Compared with those in Fig. 5, the transient changes in the potential were slower, although they were dependent on the H_2O_2 concentration. It is also noted that the output drift is smaller for 11-FUT than for FcMeOH. It has been reported that various ions adsorb on gold electrodes, e.g., halide and thiocyanate ions,[20,21] whose adsorption causes a potential change in the electrodes. In this study, the RM includes chloride ions, and thus these ions are likely to adsorb on the electrode to cause output drift in the sample with dissolved FcMeOH. On the other hand, the adsorption was less likely in the 11-FUT sample because the electrode surface was covered with 11-FUT, resulting in a smaller output drift.

The potential changes caused by the addition of H_2O_2 are plotted as a function of H_2O_2 concentration in Fig. 7, where the potential change is defined as the difference in the potential at 1500 and 280 s (after and before the H_2O_2 addition). In the sample where FcMeOH was dissolved, the concentration of FcMeOH was 2 mM, and thus, the dissolved FcMeOH could be fully oxidized with 1 mM H_2O_2, which caused the saturation behavior for H_2O_2 concentrations higher than 10^{-3} M. This result also indicates that the oxidation reaction described in Eq. (1) sufficiently proceeded in the solution. On the other hand, the output changes in the 11-FUT-immobilized electrodes were less than those for which FcMeOH was dissolved in the solution, and the limit of detection (LOD) for the 11-FUT-immobilized sample was worse. Although the potential change in the electrode is described by Eq. (3), the interaction related to charge transfer between the ferrocenes and the electrodes is necessary to cause the potential change. Thus, it is possible that the magnitude of the potential change varies depending on the state of the redox

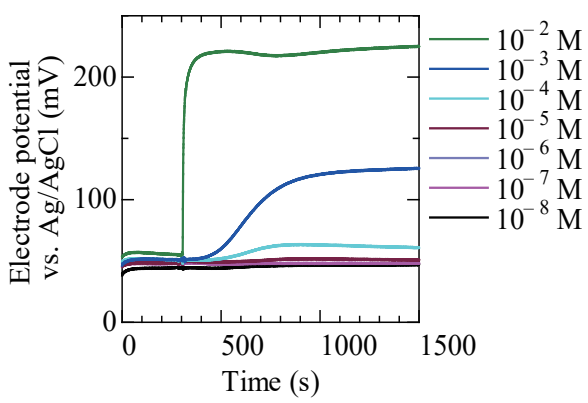

Fig. 6. (Color online) Time dependence of the potential of 11-FUT-immobilized electrode in response to the addition of H_2O_2 solution at various concentrations. The H_2O_2 solution was added at 300 s.

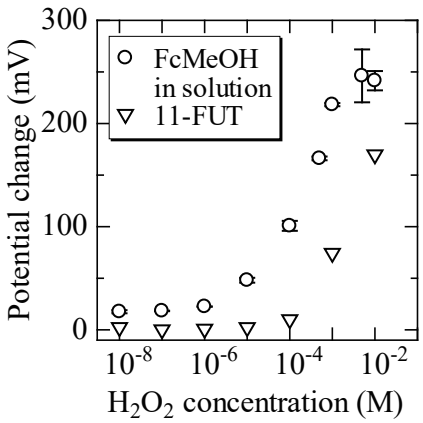

Fig. 7. Potential change caused by the H_2O_2 addition plotted as a function of the H_2O_2 concentration in the solutions.

species. In this study, the ferrocene dissolved in the solution in the form of FeMeOH moves and easily contacts with the electrode surface, whereas those immobilized on the electrode surface as 11-FUT may be restricted in their movement to sufficiently interact with the electrodes, causing the output difference. Additionally, no saturation behavior was observed above 10^{-3}-M H_2O_2. 11-FUT was immobilized with 0.5 ml of 0.5 mM 11-FUT solution. The immobilized molecules are at most 2.5×10^{-7} mol, which can be fully oxidized by 100 µl of 1.25 mM H_2O_2 solution, and the actually immobilized molecules are likely fewer than that. Thus, it is expected that the output will saturate at the lower concentration of 11-FUT than of the samples for which FeMeOH was dissolved. However, no saturation behavior was observed in the H_2O_2 concentration range of 10^{-4} to 10^{-2} M. This behavior may be related to the reaction between H_2O_2 and the ferrocenes immobilized as 11-FUT, whereas the reason of such behavior is not clear at this stage. Although further investigation on the response of the 11-FUT-immobilized device to H_2O_2 is necessary, these results demonstrate the H_2O_2 detection under biological environments by the electrodes on which electron mediators were immobilized.

4. Conclusions

In this study, potentiometric sensors were fabricated using a gold electrode and a source follower circuit. By using ferrocenes as electron mediators and HRP, the electrode potential change caused by the redox reaction including H_2O_2 was measured under biological environments. The measurements were carried out both in the samples where the mediator of FcMeOH was dissolved in the sample solutions and where 11-FUT was immobilized on the electrode surfaces. In the samples with dissolved FcMeOH, H_2O_2 was detected in the range from 10^{-5} to 10^{-3} M. On the other hand, the overall potential changes as a function of the H_2O_2 addition were lower for the 11-FUT-immobilized electrodes, and the detection range was from 10^{-4} to 10^{-2} M. Finally, it was demonstrated that H_2O_2 was detected on the basis of redox reactions with surface-modified electrodes under biological environments.

Acknowledgments

This work is partially supported by JST CREST Grant Number JPMJCR14G2, Japan and the Adaptable and Seamless Technology Transfer Program from Japan Science and Technology Agency, JST.

References

1 D. Grieshaber, R. MacKenzie, J. Vörös, and E. Reimhult: Sensors **8** (2008) 1400.
2 A. Bratov, N. Abramova, and A. Ipatov: Anal. Chim. Acta **678** (2010) 149.
3 N. Kasai, A. Shimada, N. Tobias, and K. Torimitsu: Electrochemistry **74** (2006) 628.
4 K. Y. Inoue, M. Matsudaira, R. Kubo, M. Nakano, S. Yoshida, S. Matsuzaki, A. Suda, R. Kunikata, T. Kimura, R. Tsurumi, T. Shioya, K. Ino, H. Shiku, S. Satoh, M. Esashi, and T. Matsue: Lab Chip **12** (2012) 3481.
5 J. Hasegawa, S. Uno, and K. Nakazato: Jpn. J. Appl. Phys. **50** (2011) 04DL03.
6 A. Kueng, C. Kranz, and B. Mizaikoff: Biosens. Bioelectron. **19** (2004) 1301.
7 B.-Y. Wu, S.-H. Hou, F. Yin, J. Li, Z.-X. Zhao, J.-D. Huang, and Q. Chen: Biosens. Bioelectron. **22** (2007) 838.
8 P. Bergveld: IEEE Trans. Biomed. Eng. **BME-17** (1970) 70.
9 D. G. Hafeman, J. W. Parce, and H. M. McConnell: Science **240** (1988) 1182.
10 T. Hizawa, K. Sawada, H. Takao, and M. Ishida: Sens. Actuators, B **117** (2006) 509.
11 L.-L. Chi, L.-T. Yin, J.-C. Chou, W.-Y. Chung, T.-P. Sun, K.-P. Hsiung, and S.-K. Hsiung: Sens. Actuators, B **71** (2000) 68.
12 A. B. Kharitonov, M. Zayats, A. Lichtenstein, E. Katz, and I. Willner: Sens. Actuators, B **70** (2000) 222.
13 S. Takenaga, Y. Tamai, K. Okumura, M. Ishida, and K. Sawada: Jpn. J. Appl. Phys. **51** (2012) 27001.
14 D. Braeken, D. R. Rand, A. Andrei, R. Huys, M.E. Spira, S. Yitzchaik, J. Shappir, G. Borghs, G. Callewaert, and C. Bartic: Biosens. Bioelectron. **24** (2009) 2384.
15 X.-L. Luo, J.-J. Xu, W. Zhao, and H.-Y. Chen: Biosens. Bioelectron. **19** (2004) 1295.
16 Y. Ishige, M. Shimoda, and M. Kamahori: Biosens. Bioelectron. **24** (2009) 1096.
17 Y. Ishige, S. Takeda, and M. Kamahori: Biosens. Bioelectron. **26** (2010) 1366.
18 H. Anan, M. Kamahori, Y. Ishige, and K. Nakazato: Sens. Actuators, B **187** (2013) 254.
19 S. Mizutani, Y. Okumura, T. Horio, T. Iwata, K. Okumura, K. Takahashi, Y. Murakami, F. Dasai, M. Ishida, and K. Sawada: Sens. Mater. **29** (2017) 253.
20 C. A. Melendres and F. Hahn: J. Electroanalytical Chem. **463** (1999) 258.
21 M. Bron and R. Holze: Electrochim. Acta **45** (1999) 1121.